

## Article

# A Design Proposal Using Coherently Radiating Periodic Structures (CORPSs) for 2-D Phased Arrays of Limited Scanning

Gilberto Calvillo <sup>1,\*</sup>, Marco A. Panduro <sup>1,\*</sup>, Elizvan Juarez <sup>1</sup>, Alberto Reyna <sup>2</sup> and Carlos del Rio <sup>3</sup>

<sup>1</sup> Department of Electronic and Telecommunications, CICESE Research Center, Carretera Ensenada-Tijuana No. 3918, Zona Playitas, Ensenada 22860, Mexico; gcalvillo@cicese.edu.mx (G.C.); elizvan@cicese.edu.mx (E.J.)

<sup>2</sup> Electrical and Electronic Engineering Department, Autonomous University of Tamaulipas UAMR-R, Reynosa 88710, Mexico; alberto.reyna@docentes.uat.edu.mx

<sup>3</sup> Electrical, Electronic and Communication Engineering, University Public of Navarra, 31006 Pamplona, Spain; carlos@unavarra.es

\* Correspondence: mpanduro@cicese.mx

**Abstract:** New configurations of 2-D phased arrays are proposed in this paper for reducing the number of phase shifters. This design methodology is based on the use of a novel coherently radiating periodic structures (CORPSs) block for 2-D phased arrays. Two new antenna systems for 2-D phased arrays are studied and analyzed utilizing the CORPSs blocks of four inputs and nine outputs. These CORPSs feeding blocks are applied in a smart way to feed the planar antenna arrays by generating the required phase plane and reducing the number of control ports. Interesting results are provided based on the experimental measurements and full-wave simulations. These results illustrate a great reduction of the active devices (phase shifters), providing a good design compromise in terms of the scanning range and side lobe level performance. Furthermore, the provided results illustrate a maximum reduction capability in the number of phase shifters of 81%, considering a scanning range of  $\pm 30^\circ$  in azimuth and  $\pm 30^\circ$  in elevation. A raised cosine distribution is applied to reach side lobe levels of  $-19$  dB for  $\pm 18^\circ$  and  $-17$  dB for  $\pm 30^\circ$  in elevation. These benefits could be of interest to designers of phased antenna systems.

**Keywords:** 2-D phased array; scanning; CORPS; phase shifters



**Citation:** Calvillo, G.; Panduro, M.A.; Juarez, E.; Reyna, A.; del Rio, C. A Design Proposal Using Coherently Radiating Periodic Structures (CORPSs) for 2-D Phased Arrays of Limited Scanning. *Appl. Sci.* **2024**, *14*, 8409. <https://doi.org/10.3390/app14188409>

Academic Editor: Piotr Gas

Received: 10 August 2024

Revised: 11 September 2024

Accepted: 14 September 2024

Published: 18 September 2024



**Copyright:** © 2024 by the authors. Licensee MDPI, Basel, Switzerland. This article is an open access article distributed under the terms and conditions of the Creative Commons Attribution (CC BY) license (<https://creativecommons.org/licenses/by/4.0/>).

## 1. Introduction

The antenna arrays technology has become an essential component of wireless applications [1–10]. These new wireless applications require phased antenna systems to provide the radiation requirements. However, the phased antenna systems based on antenna array structures are certainly of high complexity to generate the expected radiation. Then, more architectures of phased antenna systems based on less complex antenna arrays are necessary to accomplish the required radiation and to reduce the number of control ports or active devices [11]. This is an open problem in the state of the art.

There are several techniques cited in the literature to reduce the number of control ports (or phase shifters) in the design of phased antenna arrays. For example, these techniques consider the application of sub-arrays [11–22] to simplify the complexity of the array system. Several architectures based on sub-arrays have been analyzed in the state of the art, providing reduced scanning ranges for the radiation features of the low side lobe level.

Furthermore, the application of the technique based on coherently radiating periodic structures (CORPS) [23–27] has been important to set new design configurations to decrease the number of phase shifters in the phase antenna system. This technique based on CORPSs has been successfully applied to different structures of phased antenna arrays. These systems of CORPSs take advantage of the design configurations to generate the phase slope

or phase plane necessary for beam-scanning. Architectures of complete antenna system have been provided by these previous works in the literature.

Many design configurations have been proposed in the literature, but less complex antenna systems (and less expensive ones) are needed to fit the new wireless applications and satisfy the radiation requirements. Thus, this paper presents a design strategy using CORPSs for 2-D phased array systems of limited scanning. This design proposal utilizes a novel CORPSs network of four inputs and nine outputs with better operation features with respect to previous work [26]. The new  $4 \times 9$  feeding system incorporates crossovers and  $2 \times 3$  CORPSs networks [25] by ring-type dividers/combiners. The feeding system has been proposed to have a more stable transmission power, achieving better control of the output amplitude. This new  $4 \times 9$  structure incorporates different division and recombination nodes (ring type), reducing by 50% the number of the resistors used in the feeding system with respect to previous works. Furthermore, this new structure provides a better phase control and has a number of recombination nodes lower than conventional feeding systems, and therefore less losses by energy dissipation. This new  $4 \times 9$  CORPSs feeding network presents better features in the reflection and transmission coefficients. This is because the crossovers of the new structure have a better performance with respect to the previous  $4 \times 9$  feeding network.

Therefore, new configurations of 2-D phased arrays are proposed in this paper using a novel feeding network for reducing the number of phased shifters. The use of CORPSs blocks is illustrated for 2-D phased arrays. Two new antenna systems for 2-D phased arrays are analyzed utilizing  $4 \times 9$  CORPSs blocks. These CORPSs feeding blocks are utilized in a smart way to feed planar antenna arrays by generating the phase plane and reducing the number of control ports. Interesting results are provided based on the experimental measurements and full-wave simulations. These results illustrate a great reduction of the active devices, providing a good design compromise in terms of the scanning range and side lobe level performance. Furthermore, the provided results illustrate a maximum reduction capability in the number of phase shifters of 81%, considering a scanning range of  $\pm 30^\circ$  in azimuth and  $\pm 18^\circ$  in elevation. A raised cosine distribution is applied to reach side lobe levels of  $-19$  dB for  $\pm 18^\circ$  and  $-17$  dB for  $\pm 30^\circ$  in elevation. These benefits could be of interest to designers of phased antenna systems.

## 2. 2-D Phased Array Design

The proposed 2-D configurations are based on the use of  $4 \times 9$  CORPSs blocks to generate the required phase plane at the antenna elements level of the array system. Next, these new configurations are explained in detail.

### 2.1. Design Model for the Configurations

Two new 2-D configurations are proposed using  $4 \times 9$  CORPSs blocks, as shown in Figures 1 and 2. The array factor, considering the 2-D phased array design, is given by [28]:

$$AF(\theta, \phi) = \sum_{n=1}^N \sum_{m=1}^M I_{n,m} e^{j[kd(n-1)\psi_x + kd(m-1)\psi_y + \beta_x + \beta_y]} \quad (1)$$

where

$$\psi_x = \sin(\theta)\cos(\phi) \quad (2)$$

$$\psi_y = \sin(\theta)\sin(\phi) \quad (3)$$

$$\beta_x = -kd(n-1)\sin(\theta_0)\cos(\phi_0) \quad (4)$$

$$\beta_y = -kd(m-1)\sin(\theta_0)\sin(\phi_0) \quad (5)$$

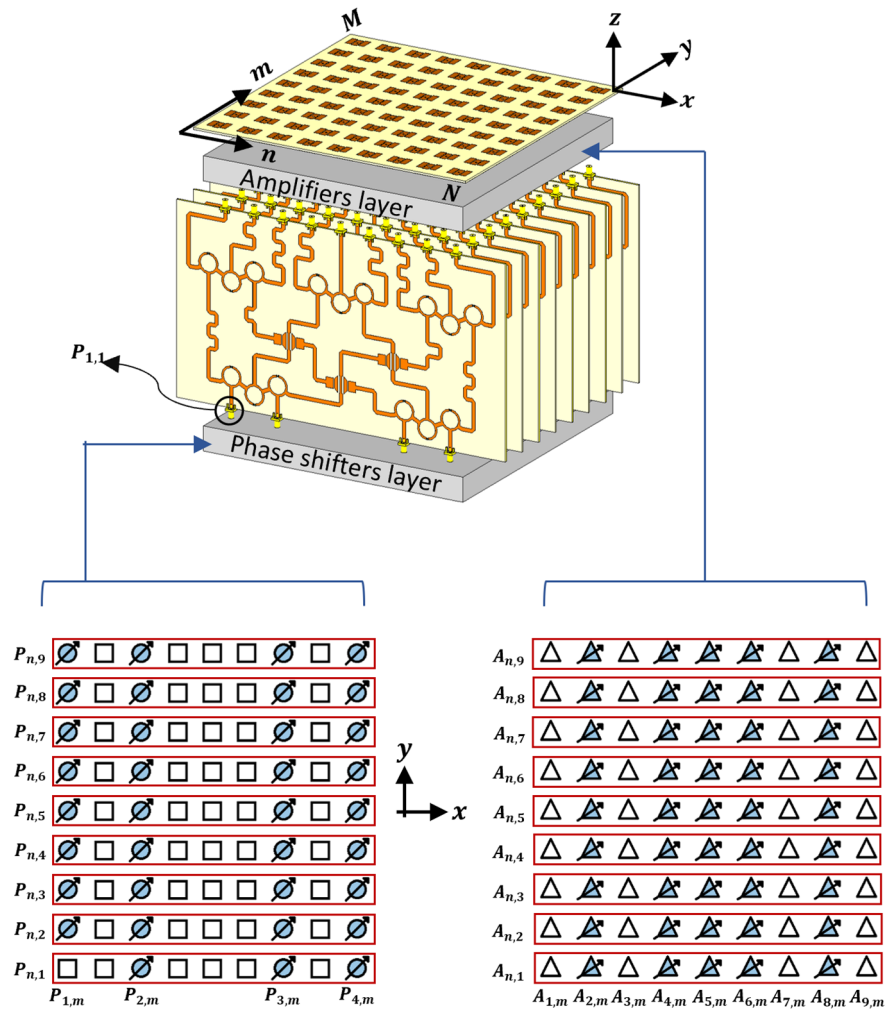


Figure 1. Design case 1 fed by 9 CORPSs blocks of 4 inputs and 9 outputs.

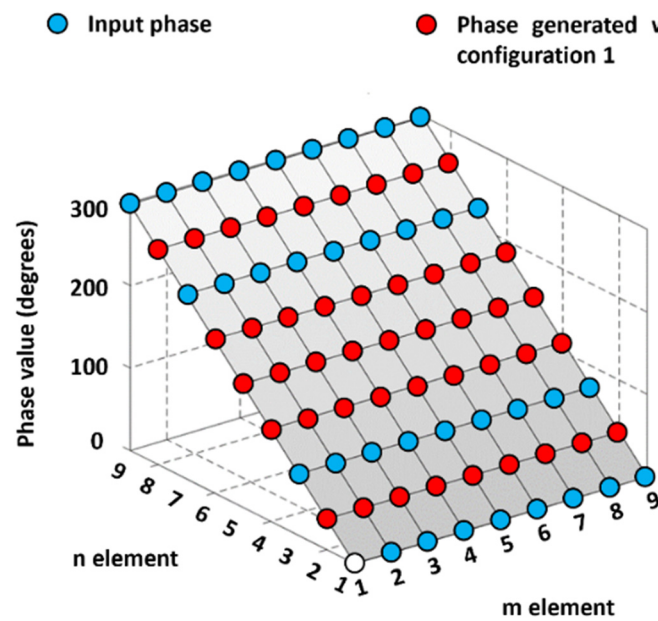


Figure 2. Phase plane generated by the design or 2-D phased array system 1.

The number of elements is defined as  $N$  over the  $x$  axis and  $M$  over the  $y$  axis, the current excitation for each  $nm$ -th antenna element is set by  $I_{nm}$ , and the phase excitation values are set by  $\beta_x$  and  $\beta_y$  at the values of  $(\theta_0, \phi_0)$  as the scanning angle.

The design case 1 (illustrated in Figure 1) utilizes 81 antennas in the 2-D phased array system. This antenna system is fed by nine CORPSs blocks of four inputs and nine outputs. This system design feeds 81 antenna elements by using 35 control ports (or phase shifters). The antenna system reduces to 57% the number of control ports or phase shifters employed in the antenna system providing beam-scanning for a range of  $\pm 40^\circ$  in azimuth and for a range of  $\pm 30^\circ$  in elevation. The amplifiers layer is connected to the output of the feeding network. The amplitude level is controlled in each antenna element. So, the raised cosine distribution can be applied to the planar array by compensating for the amplitude value generated at every output of the feeding network. The phase shifters layer is set as the first stage to control the phase flux into the network and the antenna elements. The idea is to generate the required phase plane for adequate beam-scanning. Figure 2 shows the phase plane generated by this 2-D phased array system. It is interesting to observe that by setting the input phases (blue color circles) and  $4 \times 9$  CORPSs blocks, it is possible to generate the rest of the output phases (red color circles) to build all the phase planes for beam-scanning. Every input port of the feeding system sets a phase value that permits the adequate recombination in the  $4 \times 9$  CORPSs blocks to generate the progressive phase excitation or phase plane shown in Figure 2.

The design case 2 (illustrated in Figure 3) uses two stages of  $4 \times 9$  CORPSs blocks (13 CORPSs blocks). The first stage utilizes four CORPSs blocks in order to generate 36 outputs to feed nine CORPSs blocks connected to the 81 antenna elements of the array system, i.e., 81 antenna elements are controlled by 15 phase shifters. The 2-D phased antenna system can achieve a reduction of 81% in the number of phase shifters used for a beam-scanning of  $\pm 30^\circ$  in the azimuth and  $\pm 30^\circ$  in the elevation plane. As with the previous configuration, the amplifiers layer is connected to the output of the feeding network. So, the amplitude control is operated in the same way. The phase shifters layer or phase control unit provides 15 phase values (blue color circles) to feed the first stage and to generate the rest of the output phases (red color circles) of the phase plane (81 phase values for the planar array) (see Figure 4) for beam-scanning. Please note that less control ports are required to feed the 81 antenna elements of the phased array system. As illustrated, the 2-D phased array system uses the  $4 \times 9$  CORPSs blocks to generate the required phase plane for beam-scanning using less control ports or phase shifters.

As shown previously, the outputs of the  $4 \times 9$  CORPSs blocks connect to a set of amplifiers.

Therefore, the amplification value  $A_m$  can be determined as follows:

$$A_m = \frac{I_m}{I_m} \quad (6)$$

In this design case,  $I_m$  is considered as the amplitude at the output of the feeding system and  $I_m$  is the value generated by the raised cosine amplitude distribution to obtain the desired beam with a low side lobe level. The raised cosine distribution uses the next equation to calculate the value of  $I_m$ :

$$I_m = \frac{1 + \cos\left(\frac{d_c \cos^{-1}(2a_t - 1)}{0.5L_a}\right)}{2} \quad (7)$$

where  $L_a$  is the aperture of the 2-D phased array,  $a_t$  is the taper value, and  $d_c$  is the distance value from the center of the array to the antenna element.

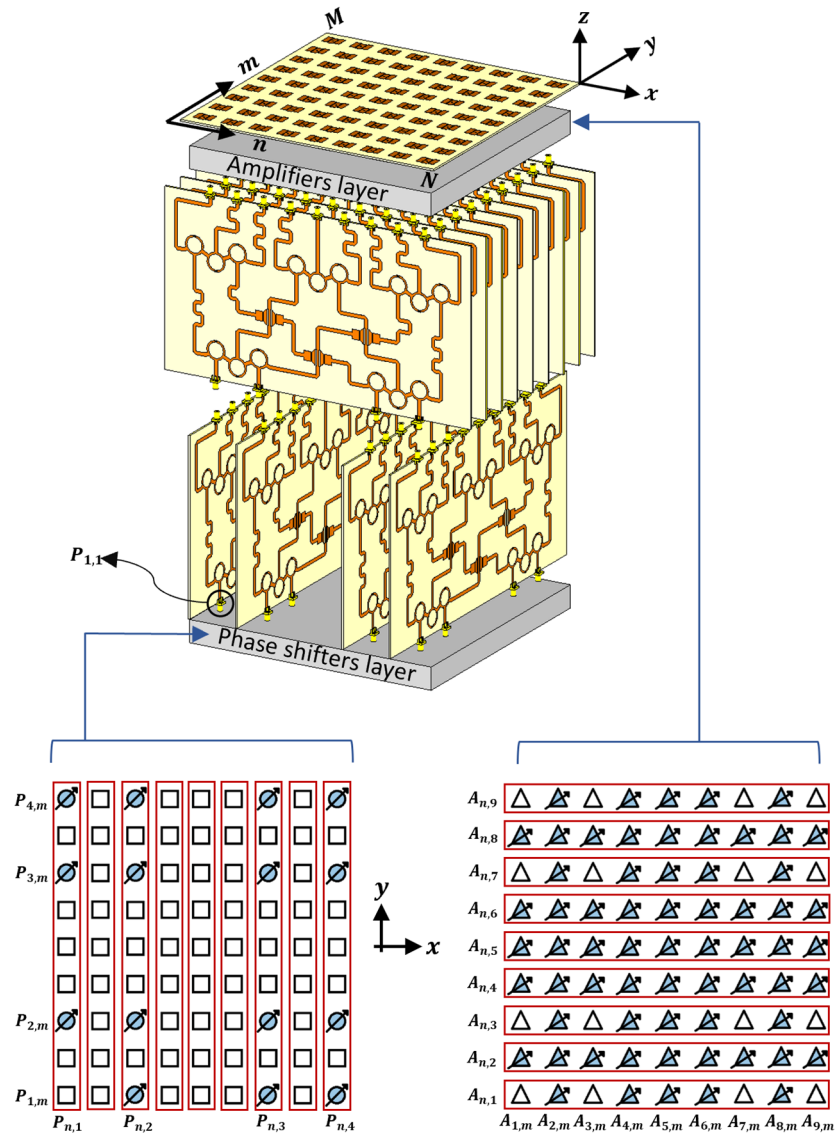


Figure 3. Design case 2 using two stages of CORPSs blocks of 4 inputs and 9 outputs.

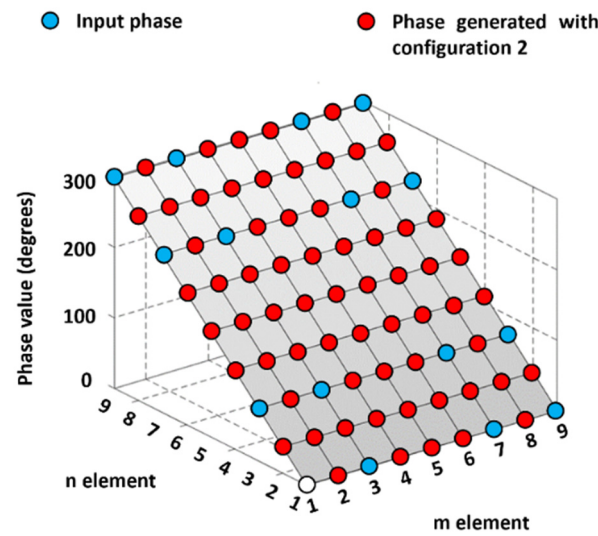
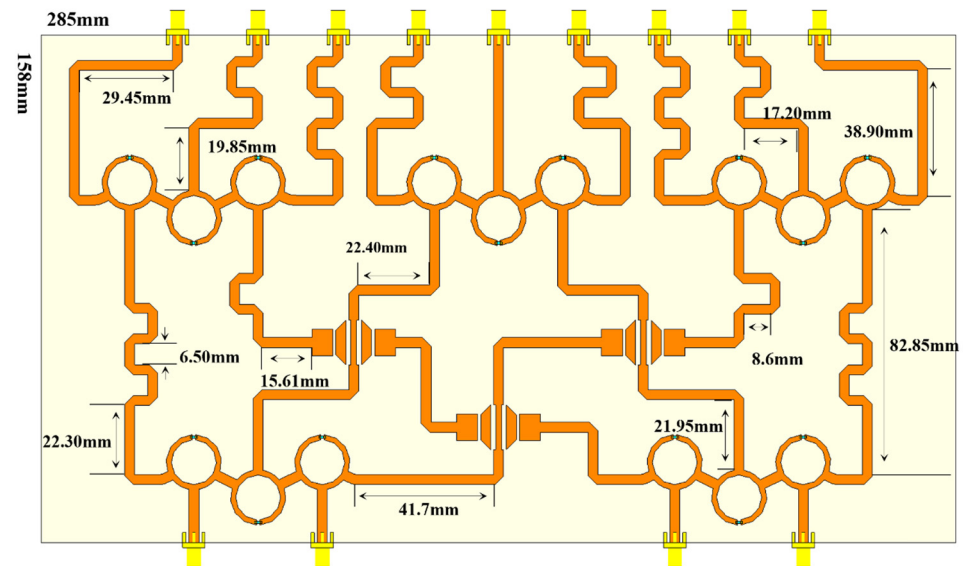


Figure 4. Phase plane generated by the design or 2-D phased array system 2.

## 2.2. Novel CORPSs Feeding System of $4 \times 9$

As set out in previous sections, the proposed 2-D configurations use  $4 \times 9$  CORPSs feeding networks to generate the required phase plane at the antenna elements and to reduce the number of phase shifters employed in the antenna system.

Figure 5 illustrates the novel feeding system based on four inputs and nine outputs using crossovers and  $2 \times 3$  CORPSs networks [25] by the ring power dividers/combiners. The dimension values of this feeding system are shown in Figure 5. This feeding system has been proposed to have a more stable transmission power, achieving better control of the output amplitude. This new  $4 \times 9$  structure incorporates different division and recombination nodes (ring type), reducing by 50% the number of the resistors used in the feeding system with respect to previous works [26]. Furthermore, this new structure provides better phase control and has a number of recombination nodes lower than conventional feeding systems, and therefore, less losses by energy dissipation. The crossovers are used in the feeding system to avoid high values of phase difference at the input ports and to make more feasible the utilization of the raised cosine distribution.



**Figure 5.** CORPSs feeding system of 4 inputs and 9 outputs, including the dimension values.

Figure 6 illustrates the behavior of the reflection coefficients (Figure 6a) and the behavior of the impedance of the feeding network system in the Smith chart format (Figure 6b). The reflection coefficients illustrate the good performance of the feeding system in a wide band with values of  $-15$  dB in the operation range of 5.5–6.0 GHz. The behavior of the impedance of the feeding network illustrates adequate values to be matched in this operation frequency range.

Figure 7 illustrates the behavior of the transmission coefficients of the novel  $4 \times 9$  feeding network. The transmission characteristics obtained are adequate, considering the losses in each element of the network system and the SMA connectors. This new  $4 \times 9$  CORPSs feeding network presents better features in terms of the reflection and transmission coefficients. This is because the crossovers of the new structure have a better performance with respect to the previous  $4 \times 9$  feeding network.

Figure 8 shows the crossover design [29] employed in the feeding network system, considering the (a) top view, (b) manufactured prototype, (c) rear view, and (d) reflection and transmission coefficients. As shown in this figure, the crossovers of the new structure have better behavior in terms of the bandwidth with respect to the previous  $4 \times 9$  feeding network. The feeding structure is sensitive to the behavior of the crossovers. The proposed crossover design helps the new  $4 \times 9$  CORPSs feeding structure to have a better performance with respect to the previous design.

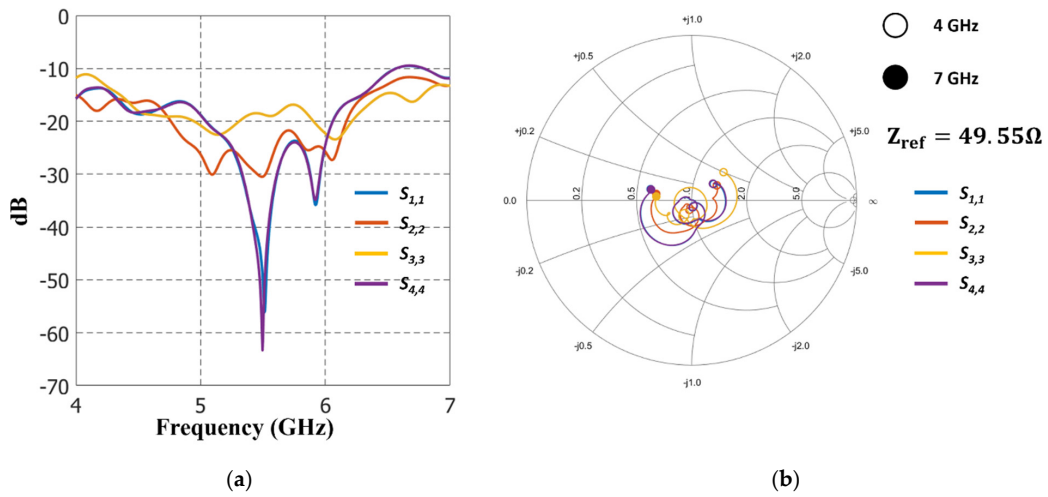


Figure 6. Behavior of the (a) reflection coefficients and the (b) match impedance of the feeding system.

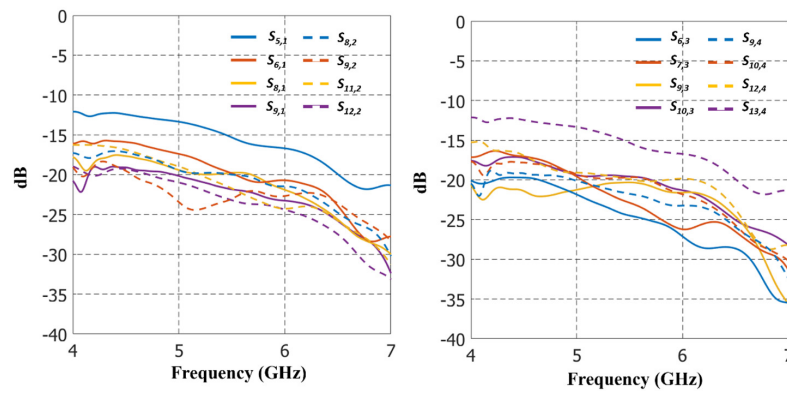


Figure 7. Behavior of the transmission coefficients of the novel  $4 \times 9$  feeding system.

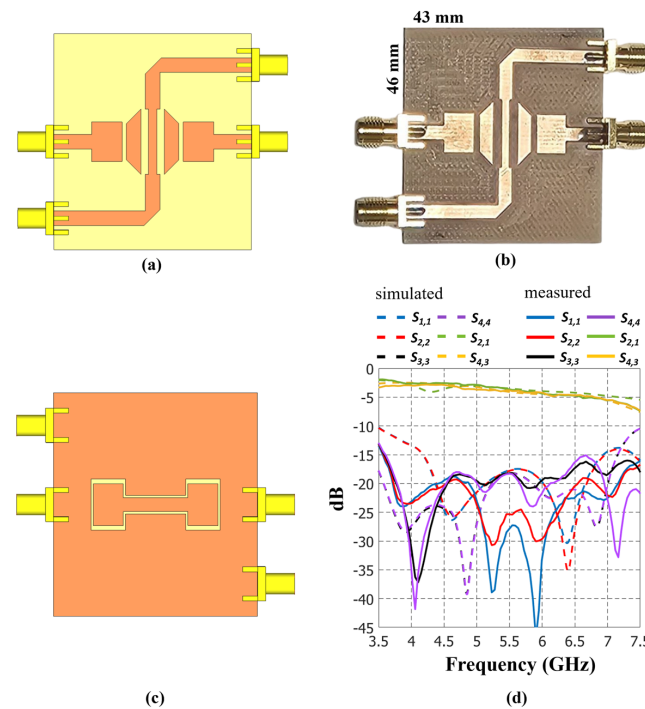


Figure 8. Crossover design of the novel  $4 \times 9$  feeding system: (a) top view, (b) manufactured prototype, (c) rear view, and (d) reflection and transmission coefficients.

Figure 9 illustrates the ring type used as a divider or combiner in the new feeding network. This ring configuration offers a compact structure and better operation features with respect to a traditional power divider [30]. The dimensions set for our configuration are shown in Figure 9b. The operation features (in bandwidth) are interesting and very adequate for the  $4 \times 9$  CORPSs feeding network and can be in observed in the behavior of the transmission and reflection coefficients shown in Figure 10.

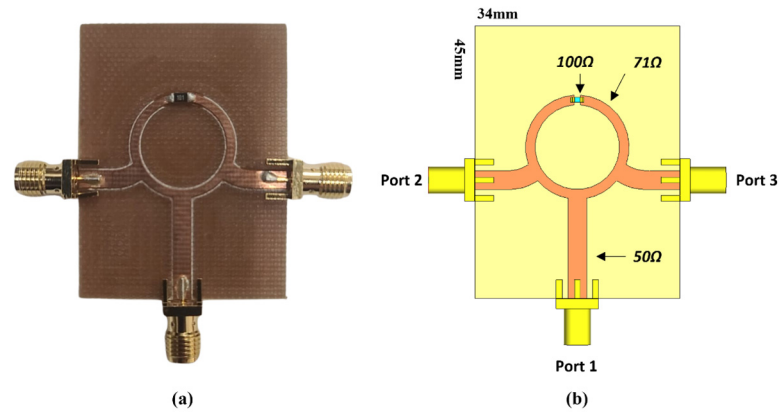


Figure 9. Division or combination node (ring type): (a) prototype and (b) design in CST with dimensions.

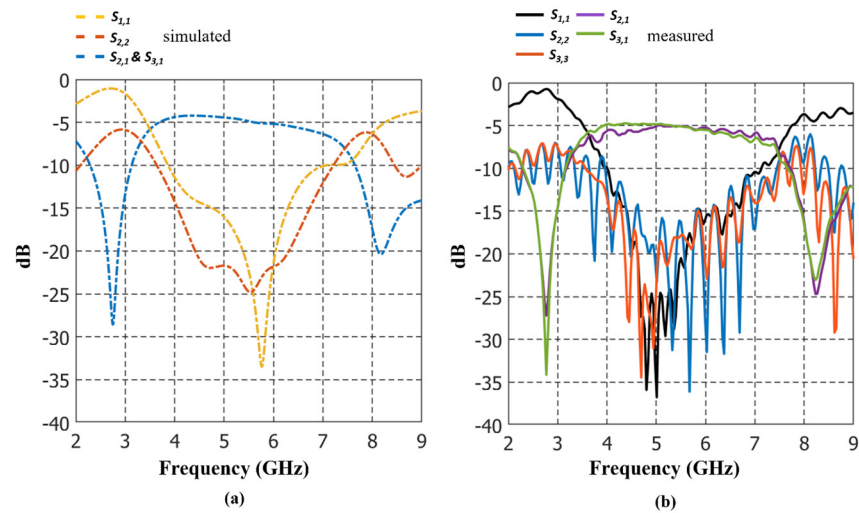
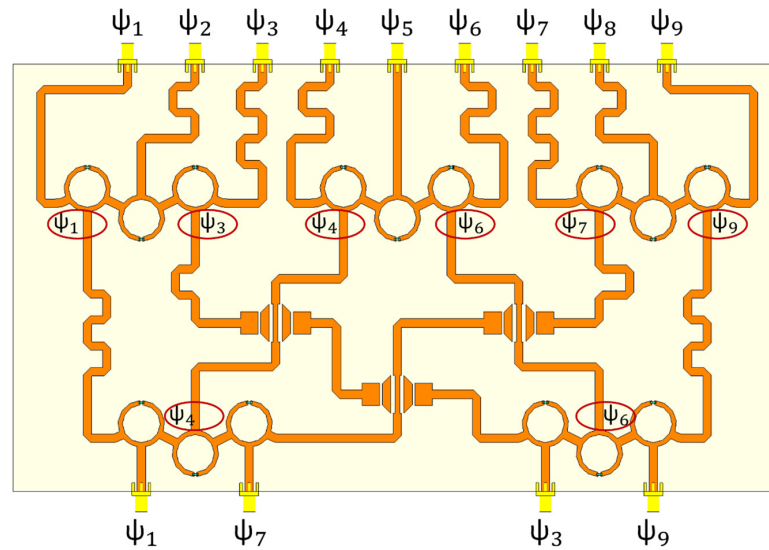


Figure 10. Behavior of the transmission and reflection coefficients for the ring-type node: (a) simulated and (b) measurements.

### Output Phase States Using Phase Control (Input PSs)

The behavior of the phase through the proposed  $4 \times 9$  feeding network is as follows. The phase values required at the outputs of the feeding system can be determined by Equations (4) and (5) given previously. Then, each block of the  $4 \times 9$  feeding system generates nine output phases (as shown in Figure 11) by using only four phase values given at the input ports. The knowledge of the phase values ( $\psi_1, \psi_3, \psi_7$ , and  $\psi_9$ ) helps to build the other output phase states ( $\psi_2, \psi_4, \psi_5, \psi_6$ , and  $\psi_8$ ) required at the antenna system. The feeding network works as a phase interpolator. The nine output phases are generated by using and knowing the value of the two extreme phases and two center phases.

For instance, Tables 1–8 illustrate several example cases of the phase values used at the input ports to generate the output phase states for different beam-scanning angles. It is interesting to observe that the phase plane (output phases of the feeding network) can be retained by adjusting the phase values of the control or input ports.



**Figure 11.** Behavior of the phase through the 4 × 9 CORPSs feeding system.

**Table 1.** Phase values at the input ports of the feeding system for ( $\theta_0 = 10^\circ$  and  $\phi_0 = 0^\circ$ ) (Conf. 2).

Block	$\psi_1$	$\psi_7$	$\psi_3$	$\psi_9$
1	0	−187.54	−62.51	−250.05
2	0	−187.54	−62.51	−250.05
3	0	−187.54	−62.51	−250.05
4	0	−187.54	−62.51	−250.05

**Table 2.** Phase values at the output ports of the feeding system for ( $\theta_0 = 10^\circ$  and  $\phi_0 = 0^\circ$ ) (Conf. 2).

Block	$\psi_1$	$\psi_2$	$\psi_3$	$\psi_4$	$\psi_5$	$\psi_6$	$\psi_7$	$\psi_8$	$\psi_9$
5	0	−31.25	−62.51	−93.77	−125.02	−156.28	−187.54	−218.79	−250.05
6	0	−31.25	−62.51	−93.77	−125.02	−156.28	−187.54	−218.79	−250.05
7	0	−31.25	−62.51	−93.77	−125.02	−156.28	−187.54	−218.79	−250.05
8	0	−31.25	−62.51	−93.77	−125.02	−156.28	−187.54	−218.79	−250.05
9	0	−31.25	−62.51	−93.77	−125.02	−156.28	−187.54	−218.79	−250.05
10	0	−31.25	−62.51	−93.77	−125.02	−156.28	−187.54	−218.79	−250.05
11	0	−31.25	−62.51	−93.77	−125.02	−156.28	−187.54	−218.79	−250.05
12	0	−31.25	−62.51	−93.77	−125.02	−156.28	−187.54	−218.79	−250.05
13	0	−31.25	−62.51	−93.77	−125.02	−156.28	−187.54	−218.79	−250.05

**Table 3.** Phase values at the input ports of the feeding system for ( $\theta_0 = 15^\circ$  and  $\phi_0 = 10^\circ$ ) (Conf. 2).

Block	$\psi_1$	$\psi_7$	$\psi_3$	$\psi_9$
1	0	−275.27	−91.75	−367.03
2	−16.17	−291.45	−107.93	−383.21
3	−48.53	−323.81	−140.29	−156.47
4	−64.71	−339.99	−156.47	−431.75

**Table 4.** Phase values at the output ports of the feeding system for ( $\theta_0 = 15^\circ$  and  $\phi_0 = 10^\circ$ ) (Conf. 2).

Block	$\psi_1$	$\psi_2$	$\psi_3$	$\psi_4$	$\psi_5$	$\psi_6$	$\psi_7$	$\psi_8$	$\psi_9$
5	0	−45.88	−91.76	−137.64	−183.52	−229.40	−275.28	−321.16	−367.04
6	−8.09	−53.97	−99.85	−145.73	−191.61	−237.49	−283.37	−329.25	−375.13
7	−16.18	−62.06	−107.94	−153.82	−199.70	−245.58	−291.46	−337.34	−383.22
8	−24.27	−70.15	−116.03	−161.91	−207.79	−253.67	−299.55	−345.43	−391.31

**Table 4.** Cont.

Block	$\psi_1$	$\psi_2$	$\psi_3$	$\psi_4$	$\psi_5$	$\psi_6$	$\psi_7$	$\psi_8$	$\psi_9$
9	−32.36	−78.24	−124.12	−170.00	−215.88	−261.76	−307.64	−353.52	−399.40
10	−40.45	−86.33	−132.21	−178.09	−223.97	−269.85	−315.73	−361.61	−407.49
11	−48.54	−94.42	−140.30	−186.18	−232.06	−277.94	−323.82	−369.70	−415.58
12	−56.63	−102.51	−148.39	−194.27	−240.15	−286.03	−331.91	−377.79	−423.67
13	−64.72	−110.60	−156.48	−202.36	−248.24	−294.12	−340.00	−385.88	−431.76

**Table 5.** Phase values at the input ports of the feeding system for ( $\theta_0 = 5^\circ$  and  $\phi_0 = 0^\circ$ ) (Conf. 1).

Block	$\psi_1$	$\psi_3$	$\psi_7$	$\psi_9$
1	0.00	−31.38	−94.13	−125.50
2	0.00	−31.38	−94.13	−125.50
3	0.00	−31.38	−94.13	−125.50
4	0.00	−31.38	−94.13	−125.50
5	0.00	−31.38	−94.13	−125.50
6	0.00	−31.38	−94.13	−125.50
7	0.00	−31.38	−94.13	−125.50
8	0.00	−31.38	−94.13	−125.50
9	0.00	−31.38	−94.13	−125.50

**Table 6.** Phase values at the output ports of the feeding system for ( $\theta_0 = 5^\circ$  and  $\phi_0 = 0^\circ$ ) (Conf. 1).

Block	$\psi_1$	$\psi_2$	$\psi_3$	$\psi_4$	$\psi_5$	$\psi_6$	$\psi_7$	$\psi_8$	$\psi_9$
1	0.00	−15.69	−31.38	−47.06	−62.75	−78.44	−94.13	−109.82	−125.50
2	0.00	−15.69	−31.38	−47.06	−62.75	−78.44	−94.13	−109.82	−125.50
3	0.00	−15.69	−31.38	−47.06	−62.75	−78.44	−94.13	−109.82	−125.50
4	0.00	−15.69	−31.38	−47.06	−62.75	−78.44	−94.13	−109.82	−125.50
5	0.00	−15.69	−31.38	−47.06	−62.75	−78.44	−94.13	−109.82	−125.50
6	0.00	−15.69	−31.38	−47.06	−62.75	−78.44	−94.13	−109.82	−125.50
7	0.00	−15.69	−31.38	−47.06	−62.75	−78.44	−94.13	−109.82	−125.50
8	0.00	−15.69	−31.38	−47.06	−62.75	−78.44	−94.13	−109.82	−125.50
9	0.00	−15.69	−31.38	−47.06	−62.75	−78.44	−94.13	−109.82	−125.50

**Table 7.** Phase values at the input ports of the feeding system for ( $\theta_0 = 10^\circ$  and  $\phi_0 = 15^\circ$ ) (Conf. 1).

Block	$\psi_1$	$\psi_3$	$\psi_7$	$\psi_9$
1	0.00	−60.38	−181.15	−241.53
2	−8.09	−68.47	−189.24	−249.62
3	−16.18	−76.56	−197.33	−257.71
4	−24.27	−84.65	−205.42	−265.80
5	−32.36	−92.74	−213.51	−273.89
6	−40.45	−100.83	−221.60	−281.98
7	−48.54	−108.92	−229.69	−290.07
8	−56.63	−117.01	−237.78	−298.16
9	−64.72	−125.10	−245.87	−306.25

**Table 8.** Phase values at the output ports of the feeding system for ( $\theta_0 = 10^\circ$  and  $\phi_0 = 15^\circ$ ) (Conf. 1).

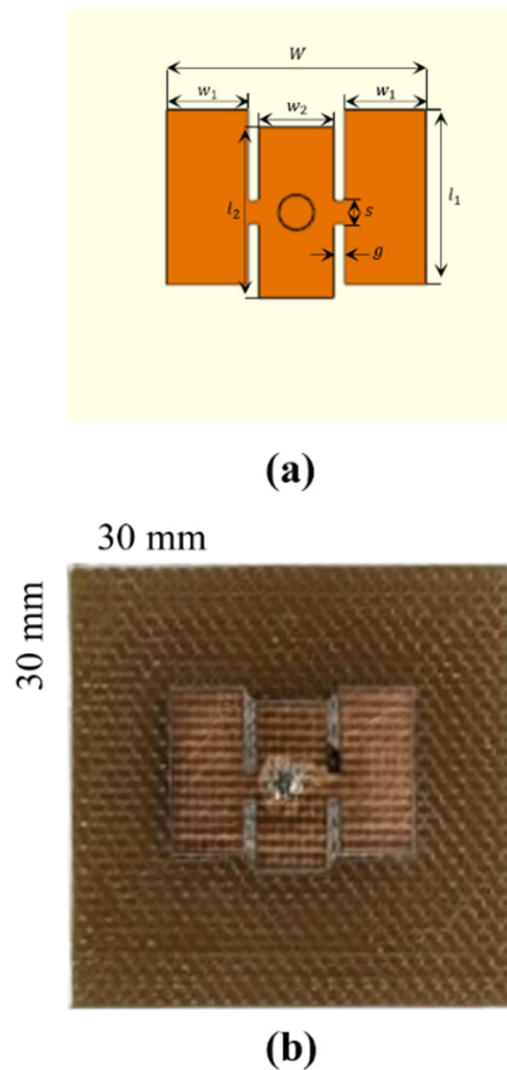
Block	$\psi_1$	$\psi_2$	$\psi_3$	$\psi_4$	$\psi_5$	$\psi_6$	$\psi_7$	$\psi_8$	$\psi_9$
1	0.00	−30.19	−60.38	−90.57	−120.77	−150.96	−181.15	−211.34	−241.53
2	−8.09	−38.28	−68.47	−98.66	−128.86	−159.05	−189.24	−219.43	−249.62
3	−16.18	−46.37	−76.56	−106.75	−136.95	−167.14	−197.33	−227.52	−257.71
4	−24.27	−54.46	−84.65	−114.84	−145.04	−175.23	−205.42	−235.61	−265.80
5	−32.36	−62.55	−92.74	−122.93	−153.13	−183.32	−213.51	−243.70	−273.89

Table 8. Cont.

Block	$\psi_1$	$\psi_2$	$\psi_3$	$\psi_4$	$\psi_5$	$\psi_6$	$\psi_7$	$\psi_8$	$\psi_9$
6	−40.45	−70.64	−100.83	−131.02	−161.22	−191.41	−221.60	−251.79	−281.98
7	−48.54	−78.73	−108.92	−139.11	−169.31	−199.50	−229.69	−259.88	−290.07
8	−56.63	−86.82	−117.01	−147.20	−177.40	−207.59	−237.78	−267.97	−298.16
9	−64.72	−94.91	−125.10	−155.29	−185.49	−215.68	−245.87	−276.06	−306.25

### 2.3. Antenna Element

The antenna element chosen to assess the 2-D phased array configurations is illustrated in Figure 12. This patch element was selected because it is easy to set and fabricate. Furthermore, it provides a wide bandwidth and good radiation characteristics, as explained in [31]. The dimension values for the design (Figure 12) are as follows:  $l_1 = 11.56$  mm,  $l_2 = 11.33$  mm,  $w_1 = 5.4$  mm,  $w_2 = 4.97$  mm,  $g = 0.73$  mm,  $s = 1.5$  mm. The current distribution (as illustrated in Figure 13) provided by the CST full-wave simulator shows that the system flux is well balanced in each antenna line. This antenna element provides good operation characteristics for the dimension values set in Figure 12.



**Figure 12.** Antenna element selected to assess the 2-D phased array systems: (a) CST design and (b) prototype.

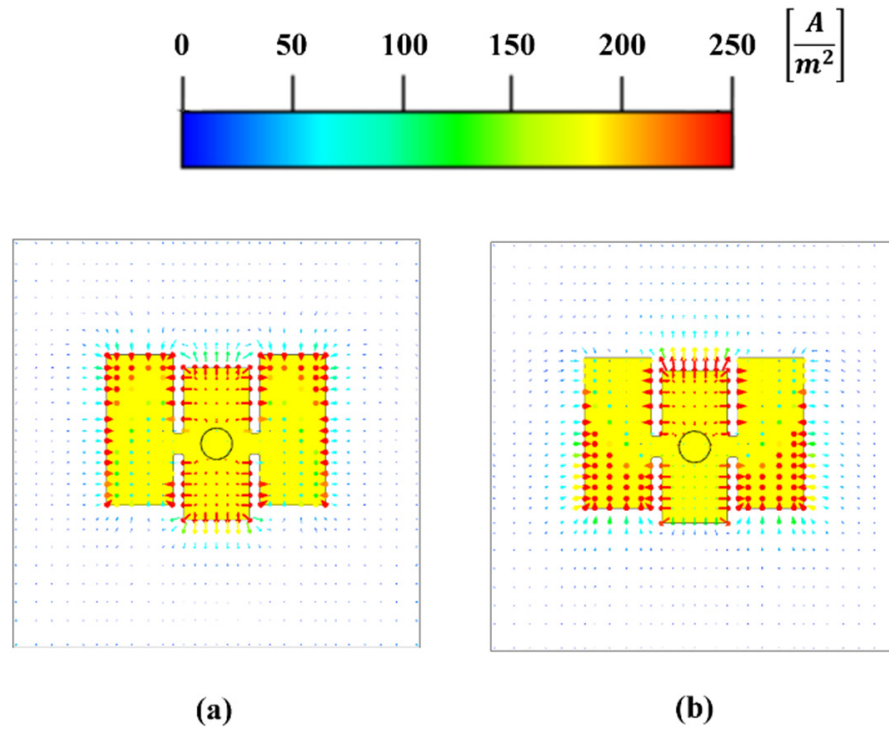


Figure 13. Current distribution of the chosen element for (a) 5.75 GHz and (b) 6.0 GHz.

Figure 14 illustrates the behavior of the reflection coefficient of the antenna element using the experimental measurements and full-wave simulations (CST solver). The chosen element achieves a bandwidth of almost 600 MHz (from 5.5 GHz to 6.1 GHz). Furthermore, the radiation pattern of the chosen element was measured in an anechoic chamber to study its behavior. Figure 15 shows the 3-D radiation pattern of the chosen antenna element using frequency cuts at 5.5 GHz, 5.75 GHz and 6.0 GHz. This antenna element provides good radiation characteristics, considering a bandwidth adequate to be applied to the 2-D phased array architectures.

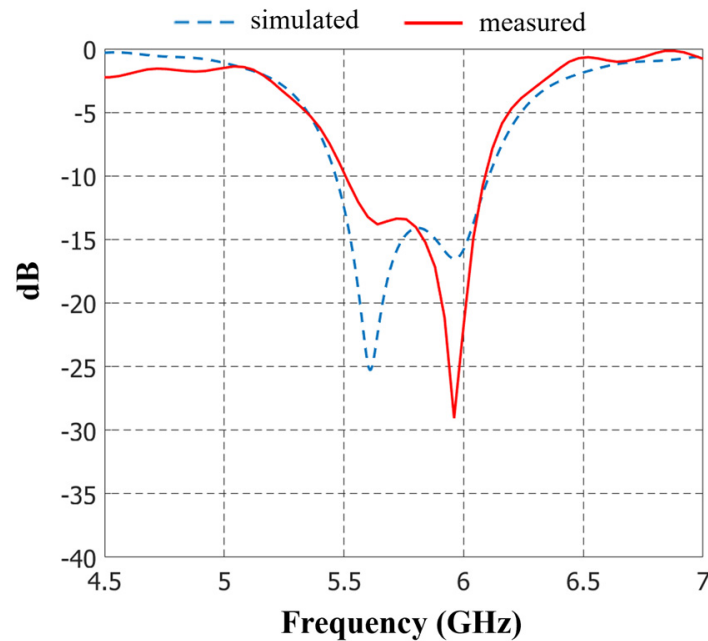
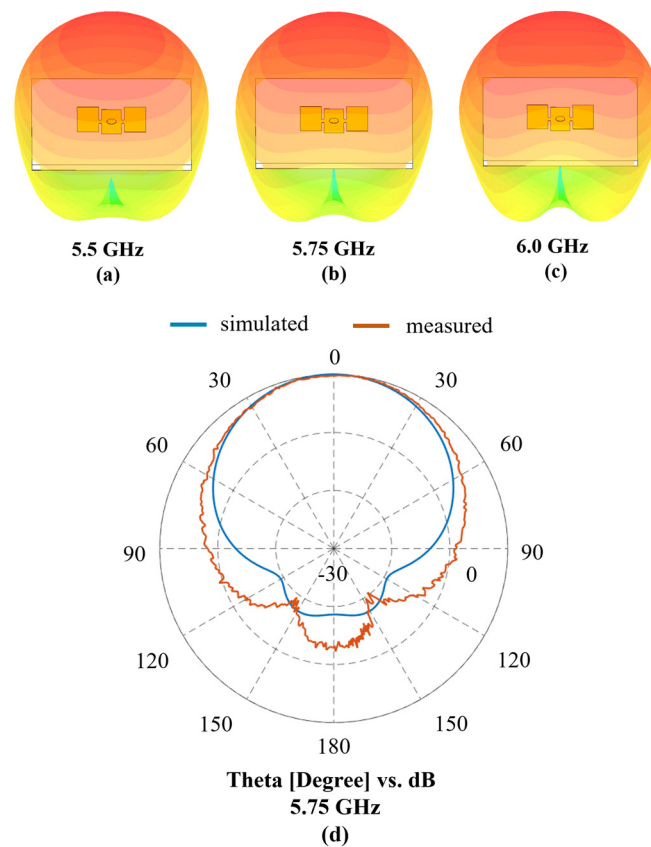


Figure 14. Behavior of the reflection coefficient of the chosen antenna element.



**Figure 15.** Radiation pattern of the chosen element obtained by the simulation (blue color) in CST and experimental measurements (red color): (a) 5.5 GHz, (b) 5.75 GHz, (c) 6.0 GHz and (d) 5.75 GHz (cut at the azimuth plane).

### 3. Full-Wave Simulation Results

The phased antenna systems based on the 2-D phased array configurations were assessed to analyze the reduction capability in terms of the number of phase shifters and beam-scanning possibilities in the planes of elevation and azimuth. The phase values were set at the input ports in order to build the phase plane in the specified direction. The 2-D phased array architectures were assessed in the CST Microwave electromagnetic solver to include mutual coupling and the errors (of amplitude and phase) caused by each proposed 2-D array configuration. CST is a reliable electromagnetic solver based on the finite integration technique.

All the simulations performed by the CST electromagnetic solver took the chosen element into account, considering the dimensions and features set in the previous section. The substrate used in the antenna element and the feeding network system was FR4. All the SMA connectors and the resistors were taken into account in the full-wave simulation. The errors of the amplitude and phase were calculated for each block of the 2-D architecture and considered at the level of the amplifiers and antenna elements of the phased array system.

Each beam-scanning angle was assessed for the two proposed 2-D architectures. Each design case (for each scanning direction) showed good matching behavior and the value of the reflection coefficient was lower than  $-10$  dB for the specified bandwidth. Figure 16 illustrates the behavior of the active reflection coefficient for the cases of the worst and best performance of the two proposed 2-D architectures. The configuration 1 presented the worst case for the farthest scanning angle.

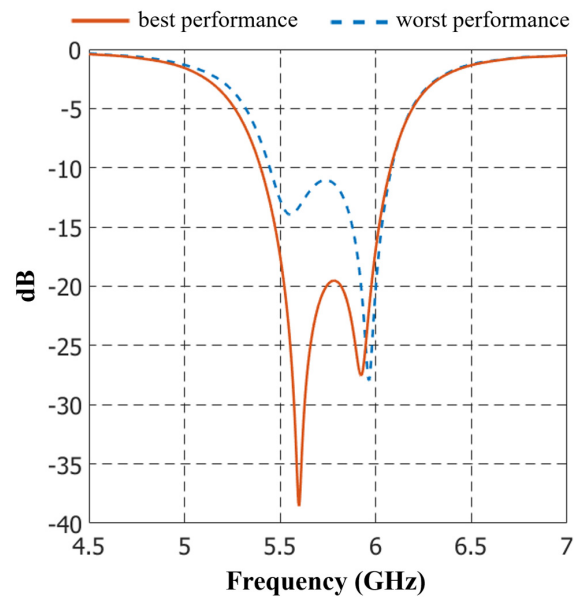


**Figure 16.** Active reflection coefficient for the cases of the worst and best performance of the two proposed 2-D architectures.

Figure 17 illustrates the 2-D phased array for the proposed antenna systems and the behavior of the 3D radiation generated using CST Microwave Studio. The cases shown in Figure 17 are as follows: (a)  $\phi_0 = 15^\circ$  and  $\theta_0 = 18^\circ$  for proposed case 2, (b)  $\phi_0 = 30^\circ$  and  $\theta_0 = 10^\circ$  for proposed case 2, (c)  $\phi_0 = 20^\circ$  and  $\theta_0 = 10^\circ$  for proposed case 1, and (d)  $\phi_0 = 40^\circ$  and  $\theta_0 = 18^\circ$  for proposed case 1. A good performance in the side lobe level was obtained for each beam-scanning angle analyzed for each proposed 2-D phased array. It reached a side lobe level performance of  $-19$  dB.

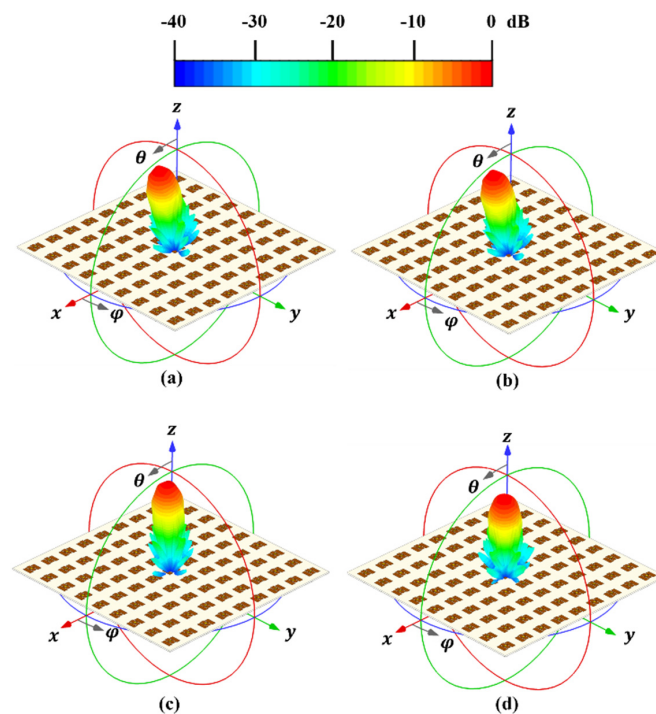


**Figure 17.** Two-dimensional phased array and 3-D radiation pattern for the proposed systems, case 2: (a)  $\phi_0 = 15^\circ$  and  $\theta_0 = 18^\circ$ , (b)  $\phi_0 = 30^\circ$  and  $\theta_0 = 10^\circ$ , case 1: (c)  $\phi_0 = 20^\circ$  and  $\theta_0 = 10^\circ$  and (d)  $\phi_0 = 40^\circ$  and  $\theta_0 = 18^\circ$ .

Figure 18 illustrates the losses in gain of the proposed antenna system, considering beam-steering. This case is generated by the proposed case 1 and a value of 1.5 dB of gain loss is generated for the proposed case 1. Therefore, good characteristics in terms of the gain and scanning performance are obtained for the 2-D phased array systems.

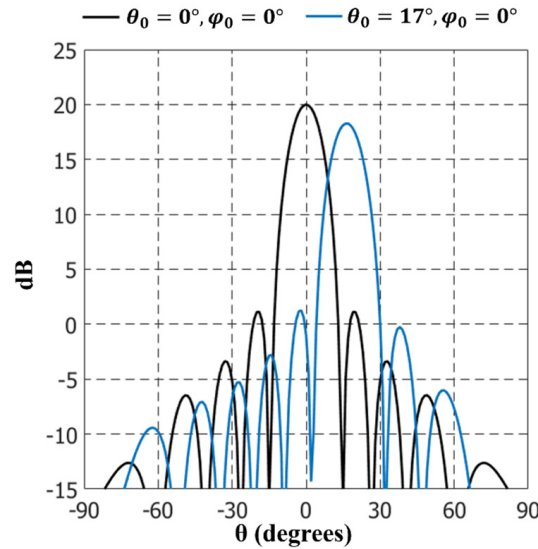


Figure 18. Worst case of the losses in gain of the proposed antenna system, considering beam-scanning.

Furthermore, Figure 19 illustrates the behavior of the radiation pattern at 5.5 GHz, 5.75 GHz and 6.0 GHz for  $\theta_0 = 18^\circ$  at the cut of  $\phi = 0^\circ$ . As observed in Figure 19, the behavior of the radiation pattern is retained if the value of frequency changes, i.e., there is no significant changes with those frequency changes.

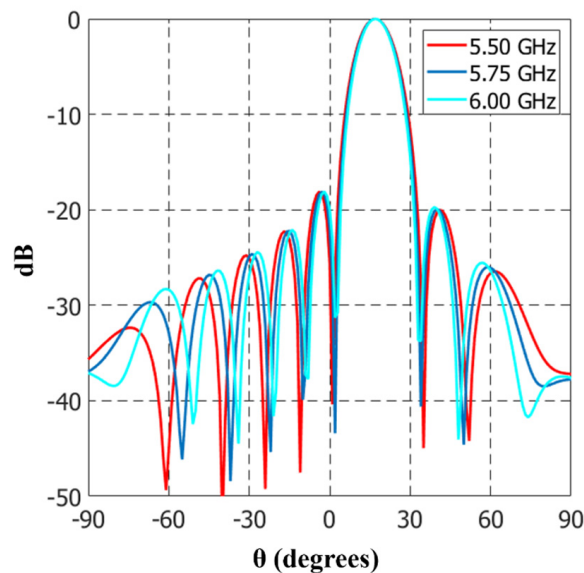


Figure 19. Behavior of the radiation pattern at 5.5 GHz, 5.75 GHz and 6.0 GHz for  $\theta_0 = 18^\circ$ .

The feeding network design can operate at  $\theta_0 = 30^\circ$  for  $\phi_0 = 0^\circ$ , as shown in the radiation pattern of Figure 20. However, there is a trade-off between the scanning angle and the amplification value (gain value of the amplifiers). It is feasible to reach this scanning angle, but high values of amplification are required, as shown in Tables 9 and 10. Furthermore, the side lobe level deteriorates to reach  $-17$  dB.

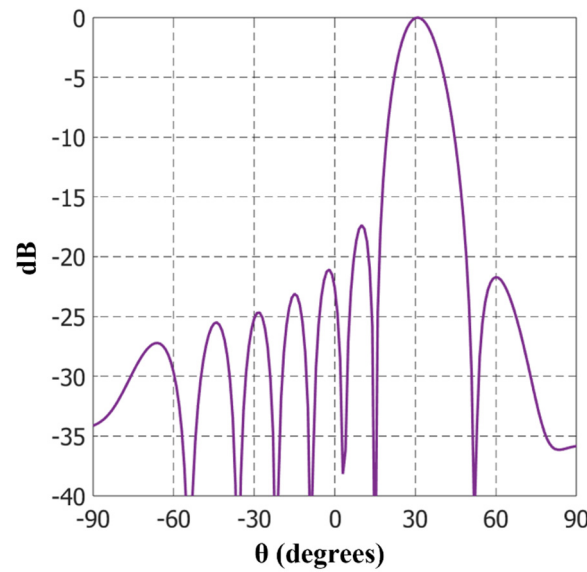


Figure 20. Behavior of the radiation pattern at the farthest scanning angle of  $\theta_0 = 30^\circ$  and  $\phi_0 = 0^\circ$ .

Table 9. Amplification values (at the outputs of the feeding system) that are required to obtain a raised cosine for  $\theta_0 = 30^\circ$  and  $\phi_0 = 0^\circ$  (Conf. 2).

	$A_{1,m}$	$A_{2,m}$	$A_{3,m}$	$A_{4,m}$	$A_{5,m}$	$A_{6,m}$	$A_{7,m}$	$A_{8,m}$	$A_{9,m}$
$A_{1,n}$	1.80	1.54	2.49	1.90	1.37	1.90	2.49	1.54	1.80
$A_{2,n}$	32.42	27.50	44.0	33.42	24.19	33.42	44.0	27.50	32.42
$A_{3,n}$	2.49	2.09	3.34	2.53	1.83	2.53	3.34	2.09	2.49
$A_{4,n}$	1.92	1.61	2.55	1.93	1.39	1.93	2.55	1.61	1.92
$A_{5,n}$	29.21	24.44	38.76	29.30	21.17	29.30	38.76	24.44	29.21
$A_{6,n}$	1.92	1.61	2.55	1.93	1.39	1.93	2.55	1.61	1.92
$A_{7,n}$	2.49	2.09	3.34	2.53	1.83	2.53	3.34	2.09	2.49
$A_{8,n}$	32.42	27.50	44.0	33.42	24.19	33.42	44.0	27.50	32.42
$A_{9,n}$	1.80	1.54	2.49	1.90	1.37	1.90	2.49	1.54	1.80

Table 10. Amplification values (at the outputs of the feeding system) that are required to obtain a raised cosine for  $\theta_0 = 30^\circ$  and  $\phi_0 = 0^\circ$  (Conf. 1).

	$A_{1,m}$	$A_{2,m}$	$A_{3,m}$	$A_{4,m}$	$A_{5,m}$	$A_{6,m}$	$A_{7,m}$	$A_{8,m}$	$A_{9,m}$
$A_{1,n}$	0.5	0.72	0.92	1.04	1.09	1.04	0.92	0.72	0.5
$A_{2,n}$	10.72	14.82	18.29	20.60	21.40	20.60	18.29	14.82	10.72
$A_{3,n}$	0.92	1.23	1.50	1.68	1.74	1.68	1.50	1.23	0.92
$A_{4,n}$	0.75	0.99	1.20	1.33	1.38	1.33	1.20	0.99	0.75
$A_{5,n}$	11.54	15.29	18.41	20.46	21.18	20.46	18.41	15.29	11.54
$A_{6,n}$	0.75	0.99	1.20	1.33	1.38	1.33	1.20	0.99	0.75
$A_{7,n}$	0.92	1.23	1.50	1.68	1.74	1.68	1.50	1.23	0.92
$A_{8,n}$	10.72	14.82	18.29	20.60	21.40	20.60	18.29	14.82	10.72
$A_{9,n}$	0.50	0.72	0.92	1.04	1.09	1.04	0.92	0.72	0.50

The interference among the antenna elements is defined by the mutual coupling between the elements. In this case, we determined the mutual coupling between different antenna elements that include different spacing between them. As you can see in Figure 21, the interference or mutual coupling between the antenna elements retained very low values. Figure 21 illustrates that the mutual coupling is higher when the distance is lower. The distance or uniform spacing (between elements) to be considered in the planar array is  $0.5 \lambda$ . This spacing helps to maintain low values of mutual coupling.

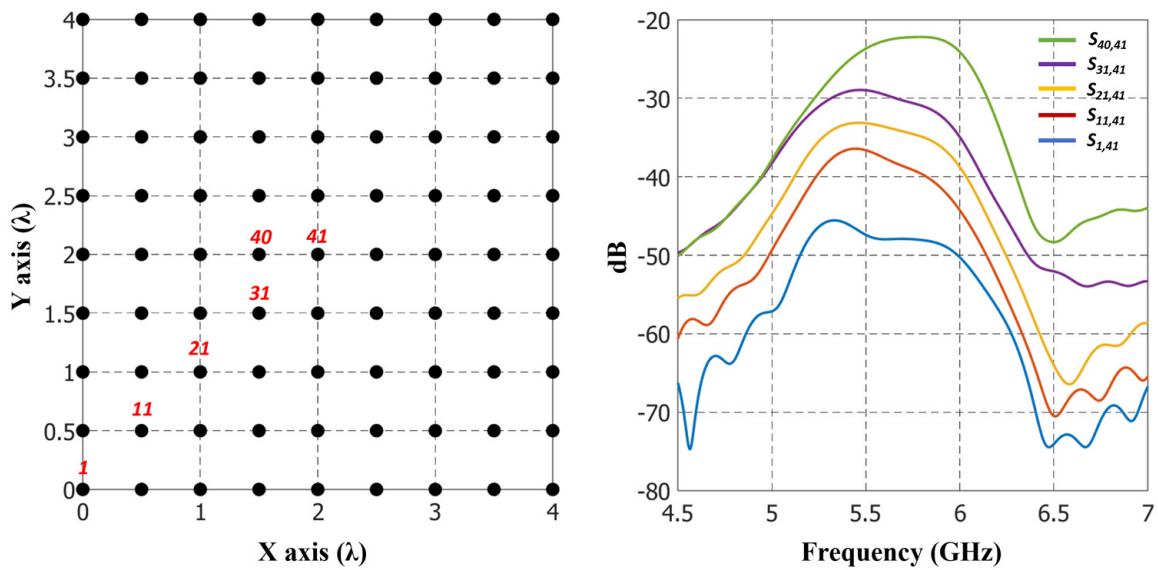


**Figure 21.** Behavior of the mutual coupling between different antenna elements (1, 11, 21, 31, 40, 41) that include different spacing between them.

Finally, Table 11 shows a performance evaluation by comparing the 2-D phased array architectures with respect to previous work, considering different methods for bi-dimensional arrays. As shown in this table, this comparison assessment analyzes the phase shifter reduction, beam-steering in azimuth and elevation, and side lobe level. It is very interesting to observe that the proposed 2-D antenna systems obtained a phase shifter reduction of 57% and 81%. These proposed configurations provide excellent design features for the reduction of phase shifters obtained in the system. These design characteristics are a side lobe level of  $-19$  dB generated by the CST electromagnetic solver (taking the mutual coupling into account) for a limited beam-scanning range, as set in Table 11. It is interesting to highlight that the proposed case 2 in this paper generates the highest reduction of phase shifters with respect to other works previously published concerning 2-D phased array systems.

**Table 11.** Performance evaluation by comparing the proposed systems with respect to previous work considering other methods.

	Number of Elements	Number of Phase Shifters	Elevation Scanning Range	Azimuth Scanning Range	Phase Shifters Reduction	Simulated Peak Side Lobe Level
Conventional phased array (raised cosine taper)	81	81	$\pm 45^\circ$	$\pm 45$	0%	$-20$ dB (AF)
This work (configuration 1)	81	35	$\pm 18^\circ$ $\pm 30^\circ$	$\pm 40^\circ$	57%	$-18.9$ dB $-17$ dB
This work (configuration 2)	81	15	$\pm 18^\circ$ $\pm 30^\circ$	$\pm 30^\circ$	81%	$-18.9$ dB $-17$ dB
Juarez et al. [25]	49	27	$\pm 25^\circ$	$\pm 40^\circ$	45%	$-19$ dB
	42	15	$\pm 25^\circ$	$\pm 25^\circ$	64%	$-19$ dB
	49	15	$\pm 25^\circ$	$\pm 25^\circ$	69%	$-18$ dB
Rupakula et al. [13]	256	60	$\pm 15^\circ$	$\pm 40^\circ$	57%	$-12$ dB (AF)
Avser et al. [18]	28	14	$\pm 24^\circ$	Not specified	50%	$-15$ dB
	28	7	$\pm 11^\circ$	Not specified	75%	$-15$ dB

More configurations can be studied and analyzed in order to generate better design solutions for 2-D phased array systems. The iterative solution of CORPSs provides more freedom degrees to split and sum the signals using less control ports. For example, our approach is based on the use of linear CORPSs blocks: the  $4 \times 9$  CORPSs block. However, planar CORPSs blocks can be designed and generated to feed in a more efficient way the architectures of 2-D phased array systems. This requires more research and analysis in the blocks of the feeding network.

Furthermore, other design techniques can be integrated with CORPSs, such as random feeding sub-arrays and interleaving systems. This can generate a complete methodology to reduce even more the phase shifters in the 2-D phased array system. In addition, the application of CORPSs and sub-arrays is particularly focused on phased antenna arrays with uniform spacing. The advantages of the antenna systems based on CORPSs can exploit the benefits of the non-uniformity of the antenna array systems. This opens more antenna design possibilities to create phased array systems with less complexity and efficient radiation characteristics. Future works will deal with these topics.

#### 4. Conclusions

New configurations of 2-D phased arrays were presented in this paper for reducing the number of phase shifters. The methodology was based on the use of a novel  $4 \times 9$  CORPSs block for 2-D phased arrays. Then, two new antenna systems for 2-D phased arrays were studied and analyzed applying CORPSs blocks of four inputs and nine outputs. The CORPSs feeding blocks were applied in a convenient manner to feed planar antenna arrays by generating the required phase plane and reducing the number of phase shifters. Full-wave simulation results were provided using an interesting antenna element for the proposed 2-D array systems. These results illustrated a great reduction of the phase shifters, providing a good design compromise in terms of scanning range and side lobe level performance.

Furthermore, the full-wave simulation results illustrated a maximum reduction capability in the number of phase shifters of 81%, considering a scanning range of  $\pm 30^\circ$  in azimuth and  $\pm 30^\circ$  in elevation. A raised cosine distribution was applied to reach side lobe levels of  $-19$  dB for  $\pm 18^\circ$  and  $-17$  dB for  $\pm 30^\circ$ . The results were compared with respect to other works previously published. The proposed cases for 2-D phased array systems provided a design solution that reaches the highest reduction of phase shifters with respect to previous work. These benefits could be of interest to designers of phased array systems.

**Author Contributions:** Conceptualization, M.A.P.; methodology, G.C.; software, G.C.; validation, G.C. and C.d.R.; formal analysis, G.C. and E.J.; investigation, G.C. and A.R.; resources, M.A.P.; writing—original draft, A.R. and G.C.; writing—review and editing, C.d.R. and A.R.; supervision, M.A.P.; project administration, E.J.; funding acquisition, M.A.P. All authors have read and agreed to the published version of the manuscript.

**Funding:** This research received no external funding.

**Institutional Review Board Statement:** Not applicable.

**Informed Consent Statement:** Not applicable.

**Data Availability Statement:** The original contributions presented in the study are included in the article; further inquiries can be directed to the corresponding author.

**Conflicts of Interest:** The authors declare no conflicts of interest.

#### References

1. Guo, Y.J.; Ziolkowski, R.W. *Advanced Antenna Array Engineering for 6G and Beyond Wireless Communications*; John Wiley & Sons: Hoboken, NJ, USA, 2021.
2. Wu, Q.; Hirokawa, J.; Yin, J.; Yu, C.; Wang, H.; Hong, W. Millimeter-wave multibeam endfire dual-circularly polarized antenna array for 5G wireless applications. *IEEE Trans. Antennas Propag.* **2018**, *66*, 4930–4935. [[CrossRef](#)]

3. Jilani, S.F.; Alomainy, A. Millimeter-wave conformal antenna array for 5G wireless applications. In Proceedings of the 2017 IEEE International Symposium on Antennas and Propagation & USNC/URSI National Radio Science Meeting, San Diego, CA, USA, 9–14 July 2017; pp. 1439–1440.
4. Godara, L.C. Applications of antenna arrays to mobile communications. I. Performance improvement, feasibility, and system considerations. *Proc. IEEE* **1997**, *85*, 1031–1060. [[CrossRef](#)]
5. Chettri, L.; Bera, R. A Comprehensive Survey on Internet of Things (IoT) Toward 5G Wireless Systems. *IEEE Internet Things J.* **2020**, *7*, 16–32. [[CrossRef](#)]
6. Marriwala, N.; Tripathi, C.C.; Kumar, D.; Jain, S. *Mobile Radio Communications and 5G Networks*; Springer: Singapore, 2021. [[CrossRef](#)]
7. Zhang, J.; Ge, X.; Li, Q.; Guizani, M.; Zhang, Y. 5G Millimeter-Wave Antenna Array: Design and Challenges. *IEEE Wirel. Commun.* **2017**, *24*, 106–112. [[CrossRef](#)]
8. Wang, Z.; Li, C.; Chen, B.; Du, H.; Song, J.; Tao, M. Research on the control technology of optical phased array high-speed scanning. *IEEE Trans. Instrum. Meas.* **2024**, *73*, 2004612. [[CrossRef](#)]
9. Mackay, A.J.; Eleftheriades, G.V. Power pattern synthesis with peripherally excited phased arrays. *IEEE Trans. Antennas Propag.* **2023**, *71*, 6390–6398. [[CrossRef](#)]
10. Xu, B.W.; Yang, Y.; Zheng, S.Y.; Che, W. Single-/Dual-beam switchable beamforming network based on phase-shifter-relaxed  $4 \times 4$  nolen matrix. *IEEE Trans. Antennas Propag.* **2024**, *72*, 518–530. [[CrossRef](#)]
11. Akbar, F.; Mortazawi, A. Scalable phased array architectures with a reduced number of tunable phase shifters. *IEEE Trans. Microw. Theory Tech.* **2017**, *65*, 3428–3434. [[CrossRef](#)]
12. Akbar, F.S.; Lighthart, L.P.; Hendrantoro, G. A toolbox of subarrays for optimizing wide-angular scanning arrays using trade-offs between scan loss and side lobe level. *IEEE Access* **2021**, *9*, 16337–16359. [[CrossRef](#)]
13. Rupakula, B.; Aljuhani, A.H.; Rebeiz, G.M. Limited scan-angle phased arrays using randomly grouped subarrays and reduced number of phase shifters. *IEEE Trans. Antennas Propag.* **2019**, *68*, 70–80. [[CrossRef](#)]
14. Oliveri, G. Multibeam antenna arrays with common subarray layouts. *IEEE Antennas Wirel. Propag. Lett.* **2010**, *9*, 1190–1193. [[CrossRef](#)]
15. Lai, F.P.; Li, H.J.; Li, C.M.; Wang, P.J.; Chen, Y.S. A multipart 5G base-station antenna using series-fed patch antenna sub-arrays. In Proceedings of the 2018 IEEE International Symposium on Antennas and Propagation & USNC/URSI National Radio Science Meeting, Boston, MA, USA, 8–13 July 2018; pp. 641–642.
16. Zhai, W.; Repeta, M.; Wessel, D.; Tong, W. mm-Wave large-scale phased array based on randomly tiled rectangular sub-arrays for 5G communications. In Proceedings of the 2017 IEEE MTT-S International Microwave Symposium (IMS), Honolulu, HI, USA, 4–9 June 2017; pp. 1895–1898.
17. Oliveri, G.; Poli, L. Synthesis of Monopulse Sub-Arrayed Linear and Planar Array Antennas with Optimized Sidelobes. *Prog. Electromagn. Res.* **2009**, *99*, 109–129. [[CrossRef](#)]
18. Avser, B.; Pierro, J.; Rebeiz, G.M. Random feeding networks for reducing the number of phase shifters in limited-scan arrays. *IEEE Trans. Antennas Propag.* **2016**, *64*, 4648–4658. [[CrossRef](#)]
19. Abbaspour-Tamijani, A.; Sarabandi, K. An affordable millimeter-wave beam-steerable antenna using interleaved planar subarrays. *IEEE Trans. Antennas Propag.* **2003**, *51*, 2193–2202. [[CrossRef](#)]
20. Avser, B.; Frazita, R.F.; Rebeiz, G.M. Interwoven Feeding Networks with Aperture Sinc-Distribution for Limited-Scan Phased Arrays and Reduced Number of Phase Shifters. *IEEE Trans. Antennas Propag.* **2018**, *66*, 2401–2413. [[CrossRef](#)]
21. Wang, D.; Hu, H.; Yang, Z. The pareto rank algorithm for the division of the subarrays for the phase array radar. In Proceedings of the 2016 9th International Congress on Image and Signal Processing, BioMedical Engineering and Informatics (CISP-BMEI), Datong, China, 15–17 October 2016; pp. 945–949.
22. Krivosheev, Y.V.; Shishlov, A.V.; Denisenko, V.V. Grating lobe suppression in aperiodic phased array antennas composed of periodic subarrays with large element spacing. *IEEE Antennas Propag. Mag.* **2015**, *57*, 76–85. [[CrossRef](#)]
23. Betancourt, D.; Bocio, C.D.R. A novel methodology to feed phased array antennas. *IEEE Trans. Antennas Propag.* **2007**, *55*, 2489–2494. [[CrossRef](#)]
24. Ferrando, N.; Fonseca, N.J.G. Investigations on the efficiency of array fed coherently radiating periodic structure beam forming networks. *IEEE Trans. Antennas Propag.* **2011**, *59*, 493–502. [[CrossRef](#)]
25. Juárez, E.; Mendoza, M.A.P.; Covarrubias, D.H.; Maldonado, A.R.; Sanchez, B.; del Rio, C. An Innovative Way of Using Coherently Radiating Periodic Structures for Phased Arrays With Reduced Number of Phase Shifters. *IEEE Trans. Antennas Propag.* **2022**, *70*, 307–316. [[CrossRef](#)]
26. Calvillo, G.; Panduro, M.A.; Sanchez, B.; Reyna, A. A New Scheme of Applying CORPS and Crossovers to Reduce the Number of Phase Shifters in Antenna Arrays. *Sensors* **2022**, *22*, 8207. [[CrossRef](#)]
27. Juárez, E.; Panduro, M.A.; Covarrubias, D.H.; Reyna, A.; del Rio, C. Application of coherently radiating periodic structures for feeding subarrays in limited-scan arrays. *IEEE Open J. Antennas Propag.* **2023**, *4*, 1154–1162. [[CrossRef](#)]
28. Balanis, C.A. *Antenna Theory: Analysis and Design*, 2nd ed.; Wiley: New York, NY, USA, 1997.
29. Abbosh, A.; Ibrahim, S.; Karim, M. Ultra-wideband crossover using microstrip-to-coplanar waveguide transitions. *IEEE Microwave Wirel. Compon. Lett.* **2012**, *22*, 500–502. [[CrossRef](#)]

30. Hammou, D.; Moldovan, E.; Tatu, S.O. Novel MHMIC millimeter wave power divider/combiner. In Proceedings of the 2011 24th Canadian Conference on Electrical and Computer Engineering (CCECE), Niagara Falls, ON, Canada, 8–11 May 2011.
31. Yoo, J.U.; Son, H.W. A Simple Compact Wideband Microstrip Antenna Consisting of Three Staggered Patches. *IEEE Antennas Wirel. Propag. Lett.* **2020**, *19*, 2038–2042. [[CrossRef](#)]

**Disclaimer/Publisher’s Note:** The statements, opinions and data contained in all publications are solely those of the individual author(s) and contributor(s) and not of MDPI and/or the editor(s). MDPI and/or the editor(s) disclaim responsibility for any injury to people or property resulting from any ideas, methods, instructions or products referred to in the content.